Performance evaluation of greenhouse ventilation strategies based on a wireless sensor network system

Shuyi Zhu[1], Shengyan Liu[1], Yinfang Song[1], Kai Li[2,3], Fen He[2,3*], Yanfei Cao[1,4*]

(1. *College of Horticulture, Northwest A & F University, Yangling 712100, Shaanxi, China*;
2. *Academy of Agricultural Planning and Engineering, Ministry of Agriculture and Rural Affairs, Beijing 100125, China*;
3. *Key Laboratory of Farm Building in Structure and Intelligent Construction, Ministry of Agriculture and Rural Affairs, Beijing 100125, China*;
4. *Key Laboratory of Protected Horticultural Engineering in Northwest, Ministry of Agriculture and Rural Affairs, Yangling 712100, Shaanxi, China*)

Abstract: Traditional ventilation control decisions for Chinese Solar Greenhouses (CSGs) rely primarily on farmers' empirical judgment. With the development of a novel ventilation system (comprising bottom vents, top vents, and back roof vents), farmers lack adequate practical experience in operating such systems. To evaluate the cooling performance of the new ventilation system in CSGs, a Wireless Sensor Network (WSN) system was established using multiple wireless temperature and humidity sensors. The Ordinary Kriging (OK) interpolation method, which was developed in LabVIEW, was employed to visualize and monitor the real-time air temperature distribution under various ventilation opening configurations and vent combinations. Additionally, the cooling amplitude and temperature uniformity were comparatively analyzed. The results indicated that the synergy of multiple vents could enhance the chimney effect, achieving efficient cooling in summer. The cooling amplitudes of the dual-vent combination (bottom vent+top vent) and the three-vent configuration were 7.1°C and 10.4°C, respectively. Increasing the ventilation area improved both the cooling effect and temperature uniformity, with more open vents and a larger top vent area offering additional benefits. The findings of this study can provide a theoretical reference for farmers to optimize greenhouse ventilation management and offer data support for the application of novel ventilation systems.

Keywords: Chinese solar greenhouse, ventilation, wireless sensor, temperature distribution, visualization
DOI: 10.25165/j.ijabe.20261903.10049

Citation: Zhu S Y, Liu S Y, Song Y F, Li K, He F, Cao Y F. Performance evaluation of greenhouse ventilation strategies based on a wireless sensor network system. Int J Agric & Biol Eng, 2026; 19(3): 110–122.

1 Introduction

With the global population projected to exceed 9 billion by 2050[1], improving food production has become one of the most critical challenges worldwide. Greenhouse cultivation is widely recognized as an effective approach to alleviating global food shortages[2]. As a leading country in protected agriculture, China accounts for 83% of the world's total greenhouse area[3] and has emerged as the largest vegetable producer globally, contributing over 50% of the world's total vegetable output. The per capita annual vegetable availability in China has reached 515 kg, 3.4 times the global average[4]. The Chinese Solar Greenhouse (CSG), a widely adopted structure in protected agriculture, provides a favorable growth environment for crops throughout the seasons, thereby enhancing yields and extending the growing period[5]. Temperature and humidity are key factors influencing crop growth; excessive levels can increase disease incidence, hinder crop development, and significantly reduce yields. Therefore, effective environmental control within CSGs is essential to ensure healthy crop growth and improve production efficiency.

Natural ventilation, as a low-cost environmental regulation method, facilitates effective energy exchange between indoor and outdoor air, exerting a significant impact on the distribution of temperature and humidity within greenhouses[6]. During transitional seasons, natural ventilation becomes the primary method for regulating temperature and humidity due to its low maintenance requirements and energy-saving advantages[7]. In winter, ventilation enhances air exchange, replenishes carbon dioxide required for photosynthesis, reduces airflow heterogeneity, minimizes localized microclimates, and removes harmful gases and excess humidity, thereby creating an optimal growing environment for crops[8]. Thus, ventilation regulation is indispensable for year-round production in CSGs.

In the field of ventilation regulation, ventilation efficiency and cooling performance have consistently been key research focuses. Since the effectiveness of natural ventilation is directly influenced by time-varying external environmental factors[9], ventilation control strategies must account for the combined effects of multiple variables and minimize control lag to achieve optimal cooling outcomes[10,11]. Numerous studies have investigated the factors influencing the natural ventilation performance of greenhouses. Regarding ventilation modes, extensive research has demonstrated

Received date: 2025-07-30 **Accepted date:** 2026-04-20
Biographies: Shuyi Zhu, MS, research interest: greenhouse environment engineering, Email: zhushuyii@163.com; **Shengyan Liu**, MS, research interest: greenhouse environment engineering, Email: liuas@nwafu.edu.cn; **Yinfang Song**, MS, research interest: greenhouse environment engineering, Email: 17399978647@163.com; **Kai Li**, PhD, Senior Engineer, research interest: greenhouse environment engineering, Email: 331897402@qq.com.
***Corresponding author: Fen He**, PhD, Senior Engineer (Professor Level), research interest: greenhouse environment engineering. Academy of Agricultural Planning and Engineering, Ministry of Agriculture and Rural Affairs, Beijing 100125, China. Tel: +86-13520595155, Email: hefen_2005@163.com; **Yanfei Cao**, PhD, Associate Professor, research interest: greenhouse structure optimization and thermal environment regulation. College of Horticulture, Northwest A&F University, Yangling 712100, Shaanxi, China. Tel: +86-18821706068, Email: caoyanfei@nwsuaf.edu.cn.

that the combination of side and roof vents generally achieves the most effective cooling in greenhouse environments[12-14]. Lyu et al. examined the effects of vent opening size, wind speed, and crop height on the microclimate within a multi-span arched plastic greenhouse under natural ventilation[15]. Zhao investigated the indoor microclimate under different combinations of three vent configurations (side vent only, roof vent only, and half-open side and roof vents) and four side vent heights (40, 60, 80, and 100 cm) in a plastic greenhouse[16].

In terms of ventilation structure, numerous studies have focused on the effects of vent size, height, and spatial arrangement on greenhouse ventilation performance. Luo conducted a study on mechanical ventilation in multi-span plastic greenhouses and proposed four structural optimization schemes by adjusting parameters such as greenhouse span, length, and the degree of door opening in the gable wall[17]. Zhang found that adding roof vents in rice seedling greenhouses can effectively improve air circulation[18,19]. The external wind direction significantly influences the airflow distribution patterns inside the greenhouse, which is consistent with previous findings[20]. It is recommended that greenhouse orientation be determined based on the dominant wind direction in the local area during construction. He et al. investigated a CSG with a detachable rear wall and employed a two-dimensional transient model to simulate indoor temperature and airflow distribution under five different sizes of rear wall vents[21]. The results indicated that a rear wall vent with a height of 1.4 m achieved the highest ventilation efficiency and the best cooling performance. Under the same ventilation area, preliminary research compared a greenhouse with front roof vents as the control group and analyzed temperature distribution under different configurations of rear slope vents. The ventilation capacity was evaluated, and several structural optimization measures were proposed[22].

In addition to greenhouse ventilation configurations, the presence of auxiliary equipment also affects natural ventilation performance. Teitel et al. demonstrated that insect-proof screens negatively impact airflow, with smaller mesh sizes resulting in lower natural ventilation efficiency[23]. Similarly, Santolini et al. found that shading nets can reduce air velocity in the crop zone to a certain extent[24].

Temperature is a critical factor influencing crop growth, development, and yield formation, with its spatial uniformity directly affecting crop growth consistency and product quality stability. In recent years, increasing attention has been paid to the uniformity of temperature and humidity distributions within greenhouses. Zhao et al. conducted a numerical simulation in a multi-span plastic greenhouse equipped with a pad-and-fan system, finding that solar radiation significantly contributes to temperature heterogeneity under mechanical ventilation, and that increasing airflow velocity can effectively reduce temperature non-uniformity in both horizontal and vertical directions[25]. Similarly, Cheng et al. simulated airflow and temperature fields in a multi-span plastic greenhouse during summer, confirming significant internal temperature gradients, with the highest temperatures occurring at the ceiling due to solar radiation[26]. Zheng et al. numerically analyzed airflow and temperature distribution in a Venlo-type glass greenhouse at varying crop heights, demonstrating that crop height significantly influences airflow velocity under natural ventilation, with taller crops leading to more pronounced temperature gradients along the greenhouse span[27]. Liu et al. implemented forced ventilation by installing fans on the rear wall of a Chinese solar greenhouse and observed that using only top ventilation, combined with forced airflow from the rear wall, unexpectedly increased greenhouse temperatures[28]. This was attributed to the closure of bottom vents, causing hot air accumulation in the upper region, which was further intensified by forced ventilation, resulting in elevated central temperatures.

Moreover, with continuous advancements in horticultural equipment, many growers lack sufficient experience with modern ventilation systems and often rely on subjective judgment for ventilation timing, leading to imprecise regulation and suboptimal performance[29,30]. Additionally, policies such as the “Guidelines on Accelerating the Development of Mechanization in Protected Cultivation” have promoted the construction of mechanization-friendly greenhouses, characterized by larger spans and higher ridge heights to accommodate machinery[31]. However, these structural changes have further exacerbated temperature non-uniformity, posing greater challenges for effective environmental control.

Nevertheless, in most studies, the overall temperature within greenhouses has often been represented by measurements taken at the geometric center or at a limited number of selected characteristic points, under the assumption of a relatively uniform temperature distribution. Several investigations have demonstrated that air temperature within greenhouses exhibits significant spatial and temporal variability[32,33]. Therefore, it is essential to move beyond single-point sensor measurements and transition from isolated point deployments to comprehensive spatial coverage. Establishing a monitoring network capable of encompassing the entire greenhouse and accurately reflecting actual environmental conditions is critical for investigating temperature and humidity uniformity as well as for achieving precise ventilation control.

The trend of modern agricultural environmental monitoring is shifting from offline systems to wireless and cloud-based data collection architectures. A Wireless Sensor Network (WSN) provides an effective solution to this problem. It offers advantages such as real-time information provision, high self-organization, and large-scale deployment, and is widely used in the environmental monitoring systems of solar greenhouses[34-36]. Furthermore, compared with traditional wired sensors, it boasts convenient installation, flexible layout, compatibility with mechanization, and low maintenance costs[37]. On the one hand, WSN can perform spatial interpolation on discrete data based on sensor measurements, enabling rapid and stable data acquisition and real-time reflection of the environmental conditions in solar greenhouses. This addresses the limitations of the Computational Fluid Dynamics (CFD) method, which has poor universality for greenhouses of different structural types and cannot promptly locate abnormal internal environmental positions[38]. On the other hand, WSN can also be integrated with Internet of Things (IoT) technology, which is of great significance for achieving automatic control of greenhouse ventilation.

In response to the aforementioned issues, this study focuses on a novel type of assembled CSG equipped with an innovative ventilation system, including bottom vents, top vents, and back roof vents. The design of this ventilation system is based on two core theories: the stack effect (thermal pressure ventilation theory) and the natural ventilation synergy effect. The stack effect posits that vertical temperature differences form air density gradients, driving hot air out of high-position vents and drawing cool air in through low-position vents[12,21]; He et al.[21] verified via CFD simulation that combining bottom and top vents with a height difference of 1.2 m can improve ventilation efficiency by 32%. The natural ventilation synergy effect emphasizes that multi-vent combinations reduce airflow resistance and expand ventilation paths to enhance overall efficiency[14,22], and Yan et al.[22] confirmed through field experiments that back roof vents can effectively alleviate top heat accumulation, providing empirical support for the three-vent combination design.

A greenhouse environment monitoring platform based on WSN was established through the deployment of 16 wireless temperature and humidity sensors. The study adopted Ordinary Kriging (OK) interpolation for temperature distribution visualization. Given the significant spatial autocorrelation of greenhouse temperature, OK interpolation can achieve optimal unbiased estimation based on the spatial distance weight of measurement points, making it more suitable for characterizing the spatial distribution of greenhouse environments than methods such as Inverse Distance Weighting (IDW). The advantages of OK interpolation in this study include adapting to sparse layouts of 16 discrete points to generate continuous temperature fields, realizing 15-minute-level real-time visualization through LabVIEW multi-threaded programming, and accurately locating high-temperature dead zones; its limitations include reliance on sensor spatial uniformity (system deviations will amplify interpolation errors). This study aims to evaluate the cooling performance and temperature uniformity distribution of the new ventilation system under varying ventilation openings and different vent combinations.

2 Materials and methods

2.1 Experimental greenhouse

The test assembled CSG is located at the horticulture farm of Northwest A&F University in Yangling, Shaanxi Province (34°16'N, 108°06'E). The external and interior views of the test greenhouse are presented in Figure 1.

a. External view

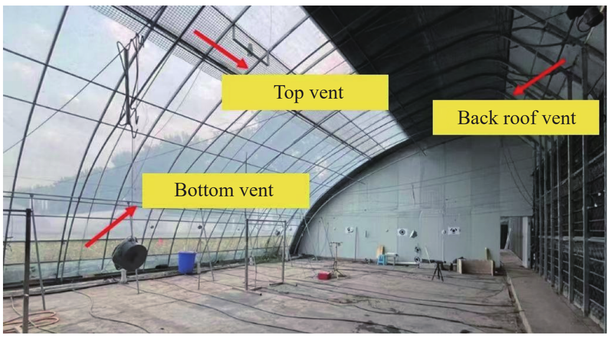

b. Interior view

Figure 1 Photos of the test greenhouse

The greenhouse has an east-west length of 15.0 m and a span of 11.0 m. The height of the rear wall is 3.6 m, and the ridge height is 5.8 m. The rear wall is constructed of water modules, and the greenhouse is equipped with a novel ventilation system comprising bottom vents, top vents, and back roof vents. The bottom vents and top vents on the front slope are installed at heights of 0.50 m and 4.78 m from the ground, respectively, with dimensions of 0.8 m in width and 15 m in length, and are opened via motorized film rolling. The back roof vents are arranged along the ridge, with a size of 8 m×2.6 m, and adopt a gear-rack system. Insect-proof nets are installed at each vent. No crops were cultivated in the greenhouse during the experimental period. The structural diagram of the test greenhouse is shown in Figure 2.

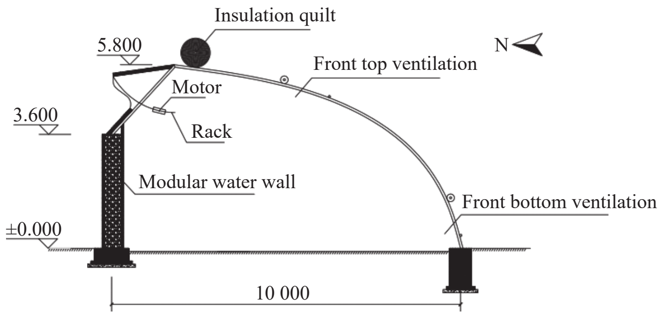

Figure 2 Test greenhouse structure diagram

2.2 Arrangement of test points

Indoor air temperature measurement points are divided into horizontal and vertical directions. Horizontal temperature and humidity measurement points are located at a height of 1.5 m in the greenhouse, arranged in a 4×4 square array, totaling 16 measurement points. The instruments used are NB-T (Narrowband Internet of Things) wireless temperature and humidity sensors (temperature measurement range: –20°C~60°C, accuracy: ±0.5°C; humidity measurement range: 0%~100%, accuracy: ±3%; manufacturer: Beijing Kunlun Coastal Technology Co., Ltd.), as shown in Figure 3. Vertical temperature measurement points are located at the geometric center of the greenhouse, at heights of 0.5, 1.5, 2.5, and 3.5 m above the ground, totaling four measurement points. T-type thermocouples (measurement range: –200°C~350°C, accuracy: ±0.2°C; manufacturer: Hezhuo (Shanghai) Wire and Cable Co., Ltd.) are used as sensors. Data are automatically recorded by a data acquisition instrument (model: 34972A, manufacturer: Agilent Technologies, USA) at 10-minute intervals.

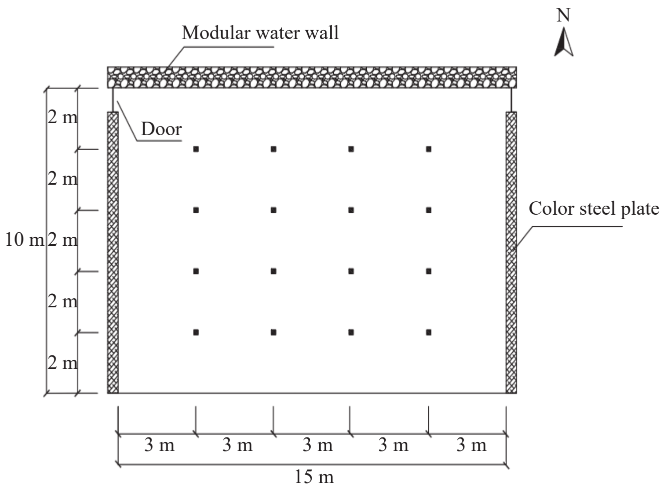

Figure 3 Distribution of temperature measurement points at 1.5 m above ground

Previous studies have shown that the number of sensors is not linearly correlated with monitoring accuracy. When the number of sensors is reduced to 16, the coefficient of determination (R^2) between estimated data and measured data is greater than 0.99, which can still meet the requirements of interpolation estimation[39].

The 4×4 square array layout of 16 sensors covers key regions of the greenhouse (including the rear wall, front edge, and central area), and the 3 m spacing between adjacent sensors ensures that monitoring data can reflect environmental changes in over 92% of the greenhouse space, balancing monitoring accuracy and equipment costs.

Outdoor environmental measurement points are located in an open area outside the greenhouse. Automatic measurements are conducted by an environmental monitoring meteorological station (temperature measurement range: –20°C to 50°C, accuracy: ±0.3°C; humidity measurement range: 0% to 100%, accuracy: ±3%; solar radiation measurement range: 0 to 1500 W/m^2; manufacturer: Beijing Huakong Xingye Technology Development Co., Ltd.) at 10-minute intervals. The detailed layout of environmental measurement points is presented in Figure 4.

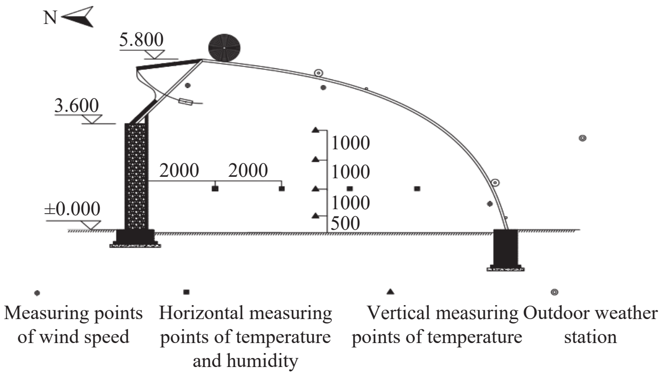

Figure 4 Side view of the test measuring points

2.3 WSN monitoring platform

The software is built based on the team's prior research, with a data flow-based application scheme and general architecture formulated. The platform consists of three main components: data collection, communication, and data analysis applications. The overall architecture of the WSN monitoring platform is shown in Figure 5.

The sensor nodes used in the test are NB-T wireless temperature and humidity transmitters. Each sensor node is equipped with functions for collecting temperature and humidity data as well as Radio Frequency (RF) communication, ensuring data independence among nodes. Meanwhile, the nodes use the RF function to communicate with the server through signal base stations, transmitting data at 15-minute intervals. The transmitted data includes temperature, humidity, timestamp, and Integrated Circuit Card Identity (ICCID) information to ensure the uniqueness of each node. The server used in the experiment is a cloud service provided by Beijing Kunlun Coastal Technology Co., Ltd. for data storage. The cloud service offers a data download interface through which ICCID, timestamp, temperature, and humidity data of sensor nodes can be obtained.

In this study, calibration and consistency testing of NB-T node sensors were conducted in accordance with the National Ecological Environment Standard (JJF 1366-2012 "Calibration Specifications for Temperature Data Acquisition Instruments"), meteorological industry standards, and metrological technical specifications. These datasets are used for data processing and analysis, and are presented to users for practical applications. The schematic diagram of the monitoring platform interface is shown in Figure 6. The software functionalities include displaying a temperature distribution heatmap inside the greenhouse, showing the area of high-temperature zones, high-temperature alarms, real-time data monitoring, and historical data query.

2.4 Data analysis methods

2.4.1 Data processing and analysis

After ensuring that the original dataset is error-free, the interpolation operation is performed on the dataset to obtain the data at 15-minute intervals, and the interpolation formula is:

$$y^* = \frac{y_n - y_m}{n - m} + y_m \tag{1}$$

where, y^* is the data within the interval, n and m are the data index values, y_n and y_m are the data interval edge-valued data values, and the interpolated data y^* range [$|y_n|$, $|y_m|$].

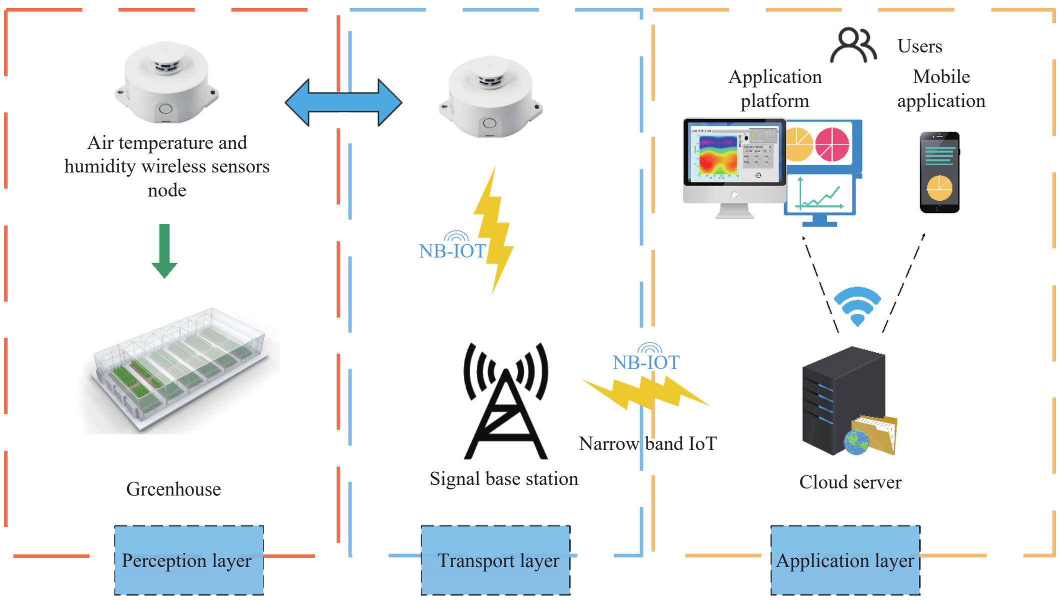

Figure 5 The overall architecture of the monitoring platform

The temperature field presented in the results section was generated using the OK algorithm based on spatial autocorrelation. Previous studies have demonstrated the effectiveness of the OK algorithm for interpolating the 2D temperature field of greenhouses[39]. The software was implemented using LabVIEW, with heatmap visualization generated based on OK algorithm interpolation results. Code was written for each functional module by dividing multiple threads in LabVIEW.

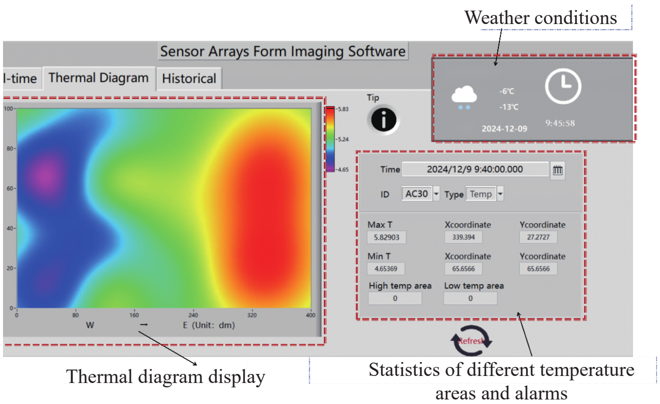

Figure 6 Schematic diagram of the monitoring platform interface

2.4.2 Temperature uniformity analysis

Temperature uniformity is one of the most important indicators for evaluating the thermal performance of greenhouses, which can be quantified by Thermal Load Leveling (TLL). TLL better reflects the temperature difference between various measurement points in the greenhouse at the same moment. TLL generally ranges from 0.40 to 0.50 or higher, and is only suitable for short-term cultivation of cold-tolerant crops like spinach and cabbage, or during transitional seasons without extreme weather periods; in greenhouses equipped with solar heating, PCM thermal storage, and other systems, TLL can be reduced to 0.20-0.36, making it suitable for year-round cultivation of warm-loving crops such as tomatoes, cucumbers, and barley. Regarding crop adaptation, warm-loving crops (including during the seedling stage) are recommended to have a long-term daily average TLL≤0.30 and a short-term TLL≤ 0.08 to avoid stress, while cold-tolerant crops can withstand TLL values of 0.30-0.40 but should avoid sustained periods over 0.45[40], defined as the ratio of the difference between the maximum and minimum temperatures in the greenhouse at that moment to their sum, calculated using the following formula:

$$\text{TLL} = \frac{T_{i,\max} - T_{i,\min}}{T_{i,\max} + T_{i,\min}} \tag{2}$$

where $T_{i,\max}$ is the maximum indoor air temperature at that moment, °C; $T_{i,\min}$ is the minimum indoor air temperature at that moment, °C.

2.4.3 Rate of temperature change analysis

To evaluate the continuous effect of different ventilation methods on indoor temperature and investigate the temperature reduction rate under different ventilation conditions per unit time, the temperature change rate[41] was introduced, calculated using the following formula:

$$R = \frac{T_{t-i} - T_i}{i} \tag{3}$$

where R is the rate of temperature change; T_i is the average temperature of the room at the moment t, °C; T_{t-i} is the average temperature of the room at the moment (t–i), °C; i is the time step, h.

2.5 Test program

The test period was from May 1, 2024 to June 30, 2024. The tested greenhouse was equipped with three types of vents: bottom vents (B), top vents (T), and back roof vents (R). In the vent opening tests, numbers were used to represent opening areas, with vents set to three states: fully open (2), half-open (1), and fully closed (0). In the vent combination tests, four opening configurations were tested: all vents closed, one vent open, two vents open, and all three vents fully open. The specific working conditions of the vents are shown in Table 1.

Table 1 Vent working conditions during vent combination tests

Opening and closing conditions	Specific working conditions
Vents fully closed	B0+T0+R0
Single vent opened	B2, T2, R2, B1, T1, R1
Double vents opened	B2+T2、B2+R2、T2+R2、B1+T1、B1+R1、T1+R1、B1+T2、B1+R2、T1+R2、B2+T1、B2+R1、T2+R1
Vents fully opened	B2+T2+R2

The test period for specific vent opening conditions was from May 23, 2024 to June 22, 2024. The working conditions and test dates for different vent opening configurations are shown in Table 2.

Table 2 Conditions of vent opening tests

Specific working conditions	Test date and weather
B0+T0+R0	May 28, cloudy
B1	May 30, sunny
T1	June 1, rainy
R1	June 7, cloudy
B2	May 26, sunny
T2	May 27, cloudy
R2	May 25, rainy
B2+T1	June 3, sunny
B2+R1	June 11, sunny
T2+B1	June 13, sunny
T2+R1	June 6, rainy
B1+R2	June 12, sunny
T1+R2	June 4, cloudy
B2+T2	June 9, sunny
B2+R2	June 2, rainy
T2+R2	June 10, sunny
B1+T2+R2	June 14, sunny
B2+T1+R2	June 17, sunny
B2+T2+R1	June 16, rainy
B2+T2+R2	May 28, sunny

The study quantified the similarity of key meteorological indicators across different dates using Pearson correlation analysis, considering three weather types: sunny, cloudy, and rainy days, as shown in Table 3.

Table 3 Similarity table of key meteorological indicators

Weather type	Key meteorological indicator	Average Pearson similarity across dates
Cloudy	Wind speed grade	0.5256
Cloudy	Radiation	0.9883
Sunny	Wind speed grade	0.7564
Sunny	Radiation	0.7147
Rainy	Wind speed grade	0.6874
Rainy	Radiation	0.9848

Note: The Pearson correlation coefficient ranges from [0, 1], where ≥0.7 indicates strong similarity, ≥0.9 indicates extremely strong similarity, and 0.5-0.7 indicates moderate similarity.

3 Results and discussion

3.1 Changes in indoor temperature and humidity in CSG in summer

The indoor temperature and relative humidity variation curves of the test greenhouse during the continuous testing period in May (May 1, 2024, 00:00-May 31, 2024, 23:59) are shown in Figure 7.

In the summer month of May, daytime temperatures were high and nighttime temperatures were low, with no significant differences in nighttime temperatures. The average indoor air temperature in the solar greenhouse was 26.5°C, the maximum temperature reached 53.3°C, and the cumulative duration of indoor air temperature exceeding 30°C accounted for 31.0% of the total time. Contrary to the temperature variation trend, humidity was lower during the day and higher at night, with an average relative humidity of 51.7%, a maximum of 87.5%, and the cumulative duration of indoor humidity exceeding 85% accounting for 2.7% of the total time. These results indicate that even with most vents open in May, indoor temperatures remain high, highlighting the need for further research on summer ventilation and cooling strategies.

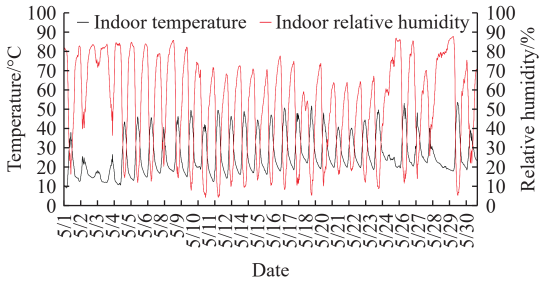

Figure 7 Variation of temperature and humidity in the greenhouse during continuous testing in May

3.2 Effect of different vent combinations on summer cooling

To investigate the cooling effect of different ventilation conditions, vents were uniformly opened at 12:00 p.m. A typical sunny day with similar external environmental conditions was selected, and the measured data at 1:00 p.m. were used to analyze the effect of different vent combinations on indoor temperature variations. Figure 8 displays the average wind speed variations (6:00-18:00) at various vents in the greenhouse during summer, both outdoors and indoors. The average wind speeds at the outdoor location, bottom vent, top vent, and back roof vent were 0.52, 0.23, 0.30, and 0.10 m/s, respectively. The maximum instantaneous wind speeds reached 2.1, 1.6, 2.4, and 1.2 m/s, with wind occurrence frequencies of 73.37%, 29.68%, 48.27%, and 16.23%, respectively.

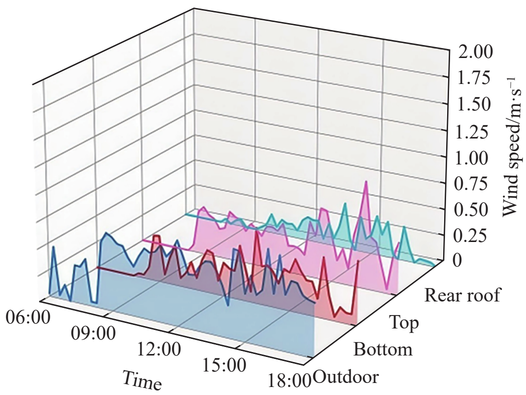

Figure 8 The average daily variation of outdoor wind speed in summer

3.2.1 Opening the single vent

Taking all vents fully closed (B0+T0+R0) as the control, three ventilation schemes were selected for comparison: bottom vent fully open (B2), top vent fully open (T2), and back roof vent fully open (R2). The test periods for each scenario were May 17th, May 20th, May 27th, and May 18th, respectively.

As shown in Figure 9, with the highest solar radiation in midday, the air temperature inside the temperature chamber also reached the highest point in the whole day. The highest indoor air temperatures of B2, T2, and R2 reached 48.1°C, 48.2°C, and 47.9°C, respectively, and the indoor air temperature without ventilation at this time was 47.8°C. After 1 h of ventilation, the average indoor air temperatures of B2, T2, and R2 decreased to 43.3°C, 41.1°C, and 43.7°C, respectively, and the temperature of B0+T0+R0 peaked at 50.7°C at the moment of 13:00 due to the absence of ventilation operation; the temperature reduction rates under each ventilation scheme were 4.8°C, 7.1°C, and 4.2°C, respectively, and the rate of cooling of T2 was higher than that of B2 and R2, respectively 2.3°C/h and 2.9°C/h, which shows that the cooling effect under T2 condition is the best.

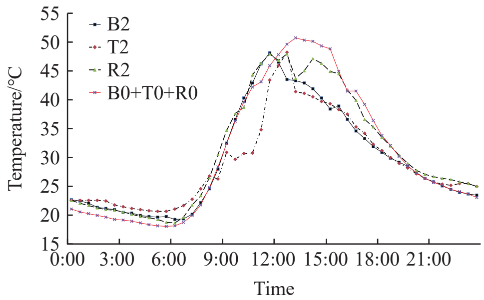

Figure 9 Daily variation of indoor temperature with a single vent open

In addition, among the three ventilation schemes, B2 had the fastest response speed, followed by T2, and finally R2. This was because the less dense hot air naturally gathers at the top of the greenhouse, and when B2 was activated, the cold air was directly blown into the interior, which drove the hot air to escape through the bottom vent. As a result, B2 exhibited the fastest cooling response, with the indoor temperature decreasing in a stepwise pattern. When T2 was activated, it directly expelled the top hot air from the top vent, and the air inlet did not interfere with the exhaust path of the hot airflow. By the time the outdoor cold air settled in the center of the greenhouse, a significant amount of indoor hot air had been expelled. Consequently, T2 showed a precipitous decrease in temperature. When R2 was turned on, the cold outdoor air entered the room through the back roof vent, causing a significant drop in indoor air temperature. Since the airflow could only exit through the back roof vent, the temperature slightly rebounded, as the air underwent exchange and mixing with the indoor and outdoor air, forming a ‘V’-shaped trough in the curve.

At 13:00, the temperature difference of B2, T2, R2, and B0+T0+R0 was 9.3°C, 6.1°C, 5.4°C, and 5.7°C, respectively, and the TLL was 0.111, 0.068, 0.064, and 0.060, respectively.

In summary, when only one vent is opened, the temperature decrease of T2 is large, the indoor temperature uniformity is better, and the cooling effect of T2 is better than that of B2 and R2.

3.2.2 Opening the double vents

Three different vent combinations: B2+T2, T2+R2, and B2+R2 were selected, and the effect of different vent combinations on the cooling effect was analyzed with all vents fully closed (B0+T0+R0) as the control. The tests were conducted on June 9, June 10, May 9, and May 17, respectively.

As shown in Figure 10, before the vents were opened, the indoor air temperatures were 49.7°C, 38.8°C, 43.5°C, and 47.8°C for B2+T2, T2+R2, B2+R2, and B0+T0+R0, respectively. After 30 min of ventilation, the indoor air temperature in the control group was 49.6°C, and the indoor air temperatures of B2+T2, T2+R2, and B2+R2 were 46.5°C, 36.7°C, and 40.2°C, which were cooled down by 3.2°C, 2.1°C, and 3.3°C, respectively. After 1 h of ventilation, at which time the temperature of B0+T0+R0 reached 50.7°C, the indoor temperatures dropped to 42.5°C, 33.5°C, and

38.2°C, respectively, cooling 7.2°C, 5.3°C, and 5.3°C. The temperature drop of B2+T2 was the largest, which was 1.9°C higher than that of both T2+R2 and B2+R2.

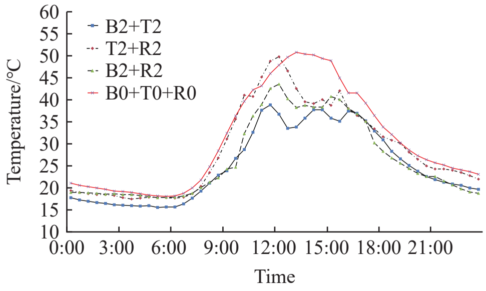

Figure 10 Daily variation of indoor temperature with two vents open

It can be seen that when both vents were opened at the same time, the cooling effect of B2+T2 was the best, which was analyzed due to the large height difference between the top and bottom vents that made it form a typical chimney effect, where the hot air was discharged from the top and the cooler air entered from the bottom, which promoted the air circulation. Secondly, the ventilation effect of B2+R2 was weakened by the possible restriction of the air intake direction of the backslope vents. Lastly, the heat pressure drive of T2+R2 was insufficient due to the small height difference formed, resulting in a lower ventilation rate and significant temperature profile fluctuations.

3.2.3 Opening all vents

As shown in Figure 11, after 30 min and 1 h of ventilation, the temperature of B2+T2+R2 decreased by 33.1°C and 29.6°C, with cooling rates of 6.9°C/h and 10.4°C/h, respectively. The 1 h temperature reduction reached 10.4°C. Analysis indicates that opening all vents provides more air circulation paths, reducing airflow resistance and enabling freer air movement, thereby increasing overall ventilation efficiency. Additionally, when all vents are fully open, the pressure distribution is more uniform, reducing the formation of eddies or dead zones and creating more effective air exchange paths with smoother airflow, thus maximizing the ventilation and cooling effect.

The results show that after vents are opened, indoor temperature drops rapidly as heat is expelled, gradually stabilizes, and then slightly rebounds under continuous solar radiation. Fully opening all vents enhances the greenhouse cooling effect and extends the cooling duration. However, during transitional seasons such as spring and autumn, when ventilation requirements are lower than in summer, a combination of vents with appropriate opening areas should be selected to achieve the desired temperature control effect. Therefore, subsequent research will further explore the cooling effect under different ventilation areas and durations to provide data reference for greenhouse vent regulation during transitional seasons, which is of great practical significance for optimizing ventilation strategies across different seasons.

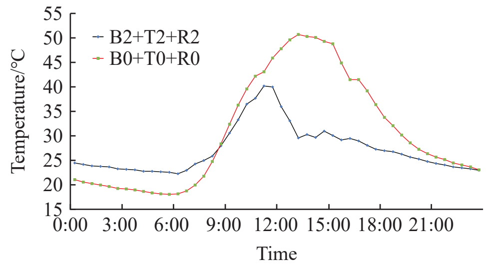

Figure 11 Daily variation of indoor temperature with three vents opened

3.3 Effect of different vent openings on summer cooling

When a single vent was opened, the bottom vent was selected to be half-open (B1) and full-open (B2) for analysis, and the test dates were June 1 and May 17, respectively. When two vents were turned on at the same time, for example, the combination of the bottom vent and the top vent, the bottom vent was fully open, the top vent was half open (B2+T1), and both the bottom vent and the top vent were fully open (B2+T2) were selected for analysis, and the testing periods were June 3 and June 13, respectively.

3.3.1 Opening the single vents

At 1:00 p.m., the horizontal plane at 1.5 m above the ground in the greenhouse after 1 h of ventilation was analyzed in Figure 12. The average indoor temperatures under the two conditions were 52.1°C and 46.2°C, respectively, and the highest temperatures appeared in the southwestern part of the greenhouse. The lowest indoor temperatures of B1 and B2 were 48.9°C and 43.3°C, respectively, and the lowest indoor temperatures of B2 were 5.6°C lower than those of B1. The difference in indoor air temperature between B1 and B2 was 6.6°C and 6.7°C, and the indoor temperature uniformity was 0.063 and 0.071, respectively. It can be seen that when the bottom vent is half-open (B1), it has little effect on the ventilation effect, and as the ventilation area increases, the cooling effect is improved, but the indoor temperature uniformity level will be slightly lower. In addition, different areas of the bottom vents have little effect on the uniformity of indoor temperature distribution.

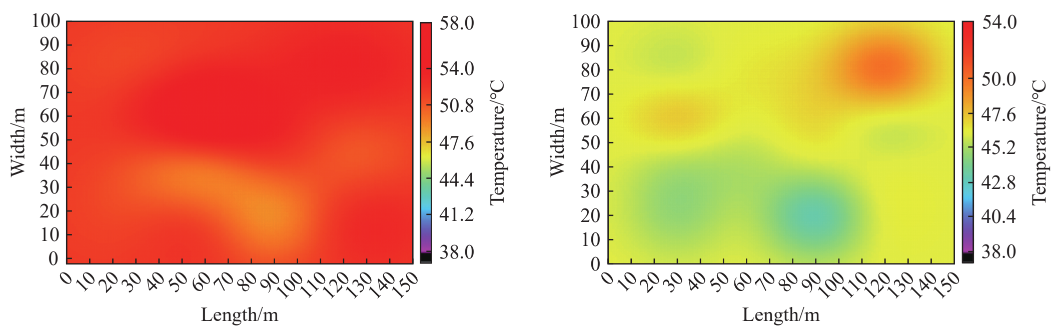

a. B1 b. B2

Figure 12 Indoor air temperature of different single-ventilation areas after 1 h of ventilation

3.3.2 Opening vent combinations

As can be seen from Figure 13, when the same vents are used, the areas with higher temperatures appear in the middle of the south end, and the areas with lower temperatures appear on both sides of the middle of the north end, and the distribution of indoor temperatures is relatively similar. The average indoor temperatures of B2+T1 and B2+T2 were 30.7°C and 33.6°C, which were higher than the outdoor temperatures by 5.0°C and 3.6°C, respectively.

The lowest indoor temperatures were 29.4°C and 32.0°C. The indoor temperature difference was 3.1°C and 3.4°C, and TLL was 0.049 and 0.058, respectively. With the increase of the ventilation area, the cooling effect of B2+T2 was obviously better, but at the same time, it also made the indoor airflow more uneven.

In summary, the larger the vent opening area, the better the cooling effect. With more air openings, the increase in vent opening area on the cooling effect is more obvious, and the impact on the uniformity of indoor airflow distribution is also more obvious.

3.4 Analysis of cooling effects under different ventilation durations

Taking the ventilation configurations with equal total opening area as an example, this study analyzed the indoor temperature variation patterns at 13:00 and 16:00 (after ventilation initiation at 12:00) for the following dual-opening combinations: B2+T1 (June 3), T1+R2 (June 4), T2+R1 (June 6), B2+R1 (June 11), B1+R2 (June 12), and B1+T2 (June 13).

Figure 14 shows the indoor air temperature cloud at different moments after turning on the ventilation for B2+T1 and B1+T2. Due to the large difference in outdoor environmental conditions between June 3 and June 13, the indoor air temperature cloud map under the two conditions differed significantly, and the highest temperature appeared in the southern part of the greenhouse near the film.

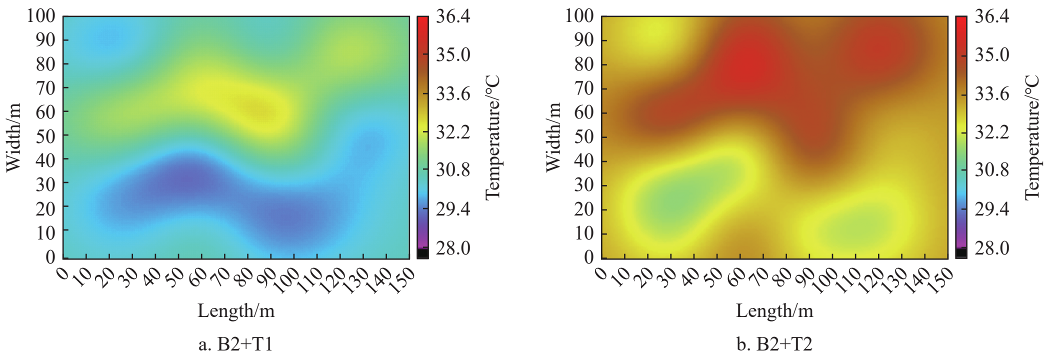

Figure 13 Indoor air temperature of different dual-ventilation areas after 1 h of ventilation

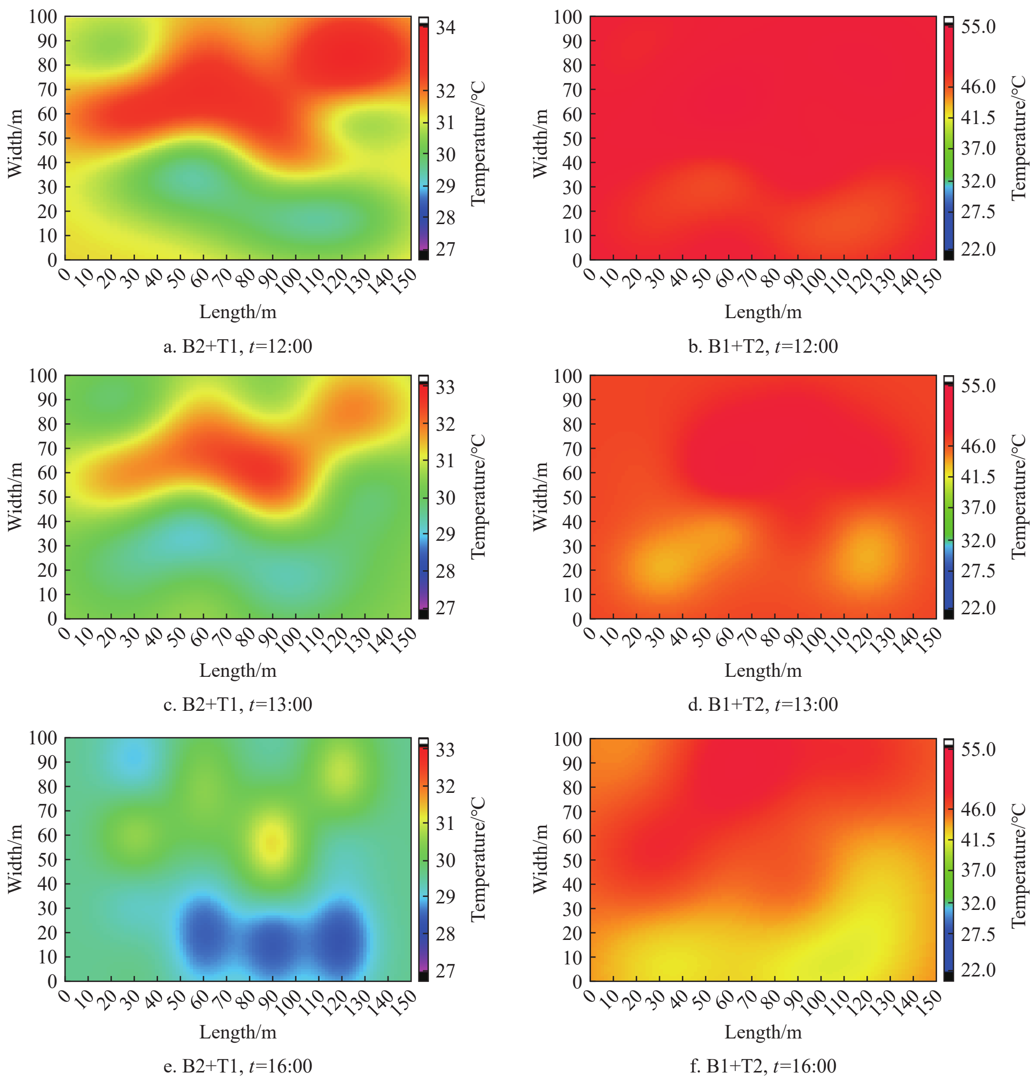

Figure 14 Indoor temperature cloud map at different moments after ventilation under B2+T1 and B1+T2 conditions

Under the condition of B2+T1, at 12:00, the average indoor air temperature was 31.3°C, the maximum air temperature was 33.3°C, the minimum air temperature was 29.7°C, the indoor temperature difference was 3.7°C, and the TLL value of the temperature uniformity index was 0.058. After 1 h of ventilation, at 13:00, the average indoor air temperature, the maximum air temperature, and the minimum air temperature were 30.7°C, 32.5°C, and 29.6°C, respectively. TLL value decreased to 0.051, and R was 0.64°C/h. At 16:00, the average, maximum, and minimum air temperatures decreased by 1.0°C, 1.3°C, and 1.0°C, respectively, compared with those at 13:00, and the TLL decreased to 0.048, and R was only 0.33°C/h in this period.

When B1+T2 was turned on, the average indoor air temperature during 12:00 to 13:00 decreased from 49.7°C to 46.8°C, with a cooling rate of 2.86°C/h. The maximum indoor temperature decreased from 53.7°C to 50.7°C, a decrease of 3.0°C, and the minimum temperature decreased from 46.2°C to 43.3°C, a decrease of 2.9°C, with the temperature difference in the room decreasing from 7.5°C to 7.4°C. The TLL increased from 0.075 to 0.079, with an uneven distribution of the indoor airflow. At 16:00, the average indoor air temperature was 45.3°C, the cooling rate was 0.50°C/h, the temperature difference was 8.1°C, and the TLL value was 0.089.

When the bottom vent and the top vent were turned on at the same time, the performances of B1+T2 and B2+T1 were the same, and the ventilation rates were fast in the early stage and slow in the later stage. During 13:00 to 16:00, the cooling rate of B1+T2 is higher than that of B2+T1 by 0.17°C/h, and the TLL value is higher than that of B2+T1 by 0.041. The cooling rate of B1+T2 is faster and larger, and the influence on the indoor airflow distribution is also larger, so it can be seen that the role of the increasing area of the top air outlet in ventilation and cooling is more obvious.

The indoor air temperature clouds at different moments after ventilation with T1+R2 and T2+R1 turned on are shown in Figure 15, and the overall air temperature distribution after ventilation still shows high in the south and low in the north.

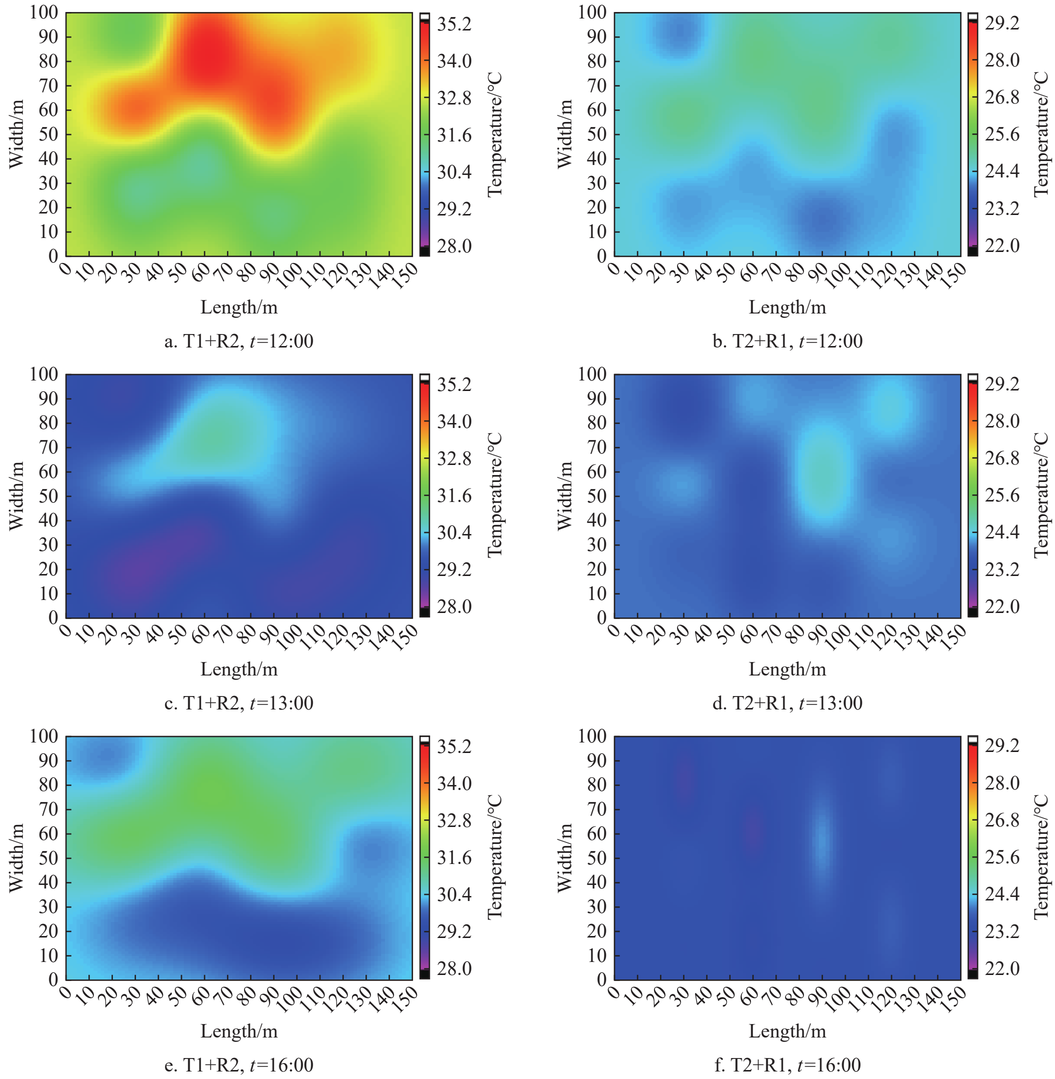

Figure 15 Indoor temperature cloud map at different moments after ventilation under T1+R2 and T2+R1 conditions

When T1+R2 was turned on at 12:00, the average indoor temperature was 32.7°C, the maximum temperature was 35.1°C, the minimum temperature was 31.0°C, and the temperature difference between the indoor temperatures was 4.1°C, with a TLL value of 0.062. After 1 h of ventilation, the average indoor temperature, the maximum temperature, and the minimum temperature were 29.6°C, 30.7°C, and 28.6°C, with a TLL value of 0.036, which was lower than that of the pre-ventilation period, at 0.026. At 16:00, the indoor temperature increased instead of decreasing; the average temperature was 30.5°C, and the TLL increased to 0.037. It could be seen that at T1+R2, the ventilation effect was good in the early stage, and R reached 3.06°C/h, but R in the later stage was not good, which might be the result of the smaller height difference leading to the outflow of fresh air in the later stage before the circulation was fully carried out. In addition, the accumulation of heat was more than the ventilation heat dissipation, which made the temperature rebound.

When T2+R1 was turned on, the overall cooling effect was seen to be insignificant. At 12:00, the average indoor temperature was 24.5°C, the highest temperature was 25.1°C, the lowest temperature was 23.9°C, the indoor temperature difference was 1.2°C, and the TLL value was 0.025. After 1 h of ventilation, the average temperature was 23.9°C, the indoor temperature difference was 1.2°C, the TLL value was 0.025, and the cooling rate was 0.59°C/h. After 4 h of ventilation, the average temperature was 23.4°C, the TLL value was 0.026, and the cooling rate was only 0.39°C/h, indicating the overall cooling effect of T2+R1. The TLL value was 0.026, and the cooling rate was only 0.39°C/h, indicating that the overall cooling effect of T2+R1 was general. It can be seen that when the top ventilation and the rear slope ventilation are opened at the same time, the overall ventilation cooling effect of both T1+R2 and T2+R1 is poor and has little effect on the uniformity of indoor air temperature, but when the rear slope ventilation is opened to a larger area, the instantaneous cooling rate is faster.

The indoor environments from June 11 to June 12 were similar, with significantly higher indoor air temperatures, and the indoor air temperature clouds at different moments after opening B2+R1 and B1+R2 for ventilation are shown in Figure 16.

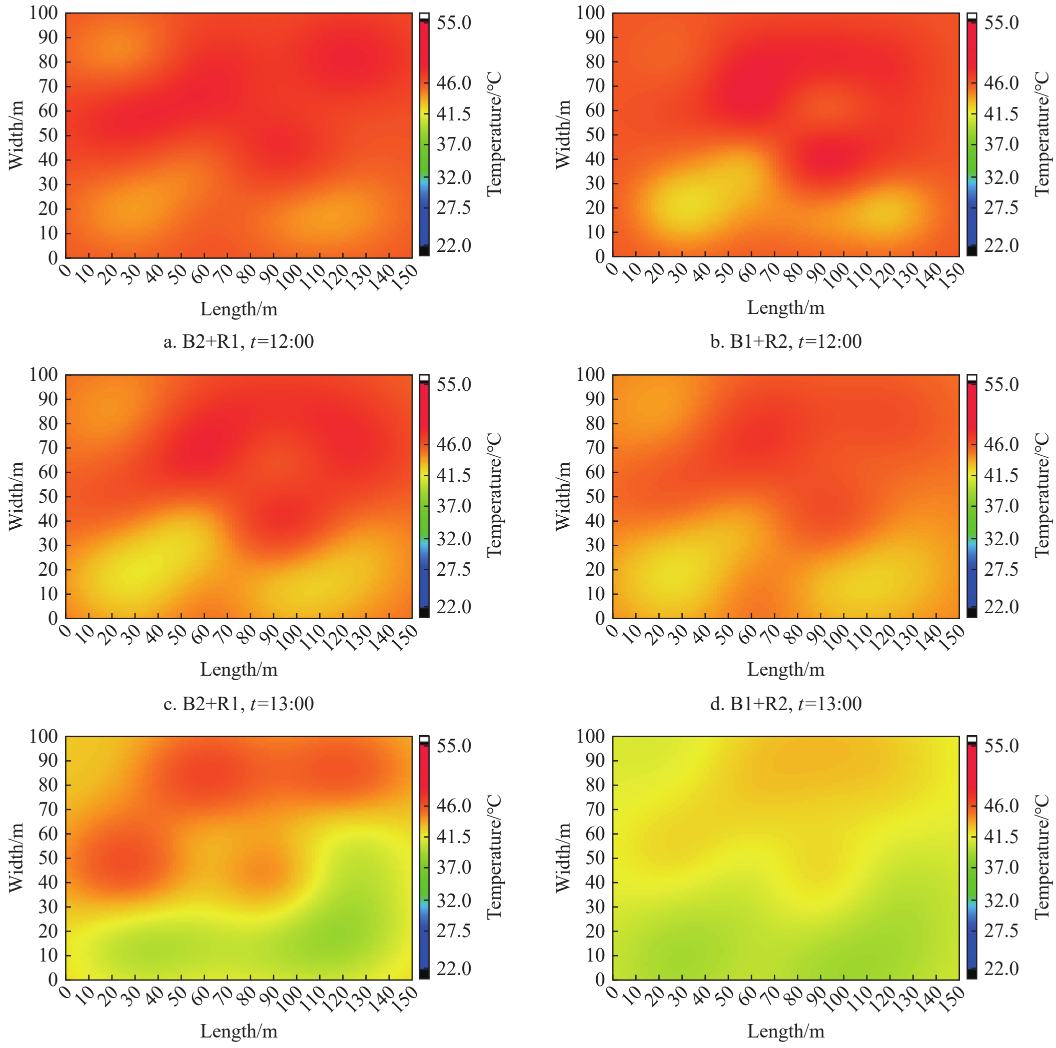

a. B2+R1, *t*=12:00
b. B1+R2, *t*=12:00
c. B2+R1, *t*=13:00
d. B1+R2, *t*=13:00
e. B2+R1, *t*=16:00
f. B1+R2, *t*=16:00

Figure 16 Indoor temperature cloud map at different moments after ventilation under B2+R1 and B1+R2 conditions

In the case of B2+R1, during 12:00 to 13:00, the average indoor air temperature decreased from 46.3°C to 45.5°C, with a cooling rate of 0.08°C/h; the minimum indoor temperature decreased from 43.8°C to 41.7°C, the indoor temperature difference increased from 4.6°C to 6.3°C, and the TLL value increased from 0.050 to 0.070. At 16:00, the average indoor temperature was 42.9°C, with a cooling rate of 0.86°C/h, a temperature difference of 7.9°C, and a TLL value of 0.093, and the airflow distribution became more uneven. At 16:00, the average indoor temperature was 42.9°C, the cooling rate was 0.86°C/h, the temperature difference was 7.9°C, the TLL value was 0.093, and the airflow distribution was more uneven.

In the case of B1+R2, during 12:00 to 13:00, the average indoor temperature decreased from 46.0°C to 44.9°C, the cooling rate was 1.05°C/h, the minimum indoor temperature decreased from 42.1°C to 42.0°C, the indoor temperature difference decreased from 6.6°C to 5.3°C, and the TLL value decreased from 0.072 to 0.059. At 16:00, the average indoor temperature was 41.2°C, the cooling rate was 0.25°C/h, the temperature difference decreased to 3.7°C, and the TLL value was 0.046.

When the bottom vent and the back roof vent were opened at the same time, the pre-cooling speed of B2+R1 was slow and the post-cooling speed was faster, but the overall temperature difference in the greenhouse was larger, the airflow distribution was more uneven, the pre-cooling speed of B1+R2 was fast at 1.05°C/h, and the post-cooling speed was slower, but the indoor airflow distribution was more even. When opening the bottom vent and the back roof vent at the same time, under the condition of equal vent opening areas, increasing the opening area of the back roof vent results in greater instantaneous cooling amplitude and more uniform overall indoor airflow distribution.

In summary, the cooling rates among different ventilation schemes under different ventilation durations varied considerably. And in terms of summer cooling, the ventilation of B1+T2 and B1+R2 had the best cooling effect.

3.5 Discussion

This study focuses on the effects of different ventilation schemes on the indoor air temperature of solar greenhouses under high summer temperatures, mainly exploring the impacts of different vent combinations, opening areas, and ventilation durations on greenhouse summer cooling. The test results show that: under the same ventilation area, when only one vent is open, the cooling performance ranks as follows: top vent>bottom vent>back roof vent; when two vents are open simultaneously, combinations with a larger height difference can form a typical chimney effect, promoting air circulation and enhancing natural ventilation efficiency, with cooling performance ranking as follows: bottom vent+top vent>bottom vent +back roof vent>top vent+back roof vent; the ventilation and cooling effect is most significant when all three vents are open. Additionally, with the increase in vent opening area and ventilation duration, the cooling effect improves, but the TLL value decreases, which is consistent with previous research findings[41].

He et al. proposed that vents are a key factor affecting greenhouse temperature distribution, and different rear wall vent areas result in different indoor airflow patterns, influencing the ventilation and cooling effect[21]. When the height of the rear wall vent is 1.8 m and 2.2 m, the ventilation area is larger, and the initial temperature drop is the fastest when the external wind direction is south (directly blowing toward the rear wall). However, continuously increasing the rear wall vent area not only does not significantly improve the ventilation efficiency of the solar greenhouse but also increases convective heat loss within the greenhouse. Thus, the ventilation area does not need to increase indefinitely; instead, a ventilation method that balances heat preservation and cooling performance should be sought. This study reached a similar conclusion that a larger vent opening area leads to a better cooling effect. Furthermore, with more vents open, the increase in ventilation area has a more pronounced effect on improving the cooling effect and a more significant impact on the uniformity of indoor airflow distribution. The overall cooling effects of both T1+R2 and T2+R1 are poor, with little impact on indoor air temperature uniformity. However, when the back roof vent is opened to a larger area, the instantaneous cooling rate is faster, which can be used for dehumidification in winter, consistent with previous research findings.

B2+R1 and B1+R2 exhibit opposite performance in early and late ventilation rates: a larger bottom vent opening area results in a faster later-stage cooling rate, while a larger back roof vent opening area leads to a faster initial cooling rate. B1+T2 and B2+T1 show similar performance, with fast early-stage ventilation rates and slow later-stage rates, but B1+T2 achieves a faster and larger cooling rate, with a more significant impact on greenhouse airflow distribution. This indicates that increasing the opening area of the top vent has a more pronounced effect on ventilation and cooling.

Table 4 systematically compiles the measured cooling rates under different ventilation combinations, opening degrees, and durations. Based on this table, ventilation recommendations are proposed as follows: 1) Extreme cooling scheme: When the greenhouse experiences extreme high temperatures on sunny afternoons in summer with the outdoor temperature continuously exceeding 33°C, the priority is to achieve rapid and significant cooling to prevent crop heat damage. At this point, the extreme cooling scheme should be adopted, involving fully opening the three sets of vents (bottom, top, and back roof: B2+T2+R2). Field measurements show that this configuration can achieve a cooling amplitude of up to 10.4°C within 1 h, exhibiting the most significant cooling effect. It is recommended to operate this mode intensively for 1-2 h to alleviate the temperature crisis before switching to a more economical ventilation mode. 2) Efficient and balanced cooling scheme: For common high-temperature periods in summer or hot days during transition seasons, it is necessary to balance efficient cooling with temperature uniformity, as well as the trade-off between effect and energy consumption. Under such circumstances, the efficient and balanced cooling scheme is recommended, i.e., fully opening the bottom and top vents (B2+T2). This configuration can leverage the significant "stack effect" to achieve a cooling of 7.2°C within 1 h, while maintaining the Thermal Load Leveling (TLL) index at an optimal level of approximately 0.058, making it suitable as the main ventilation mode in summer. 3) Energy-saving and precise scheme: When in nighttime, early morning, or cloudy weather, the focus of regulation is on low-energy-consumption precise control, aiming at mild cooling, removing accumulated heat at the top, or dehumidification and ventilation. The energy-saving and precise scheme is most appropriate here, which only involves fully opening the top vent (T2). Relying on natural ventilation by thermal pressure, this scheme has extremely low energy consumption and can still achieve a considerable cooling of 7.1°C within 1 h, adapting to management periods with low cooling demands.

Table 4 Data summary table of cooling rates under different ventilation configurations

Ventilation category	Specific ventilation mode	Observation period	Average cooling rate/°C·h^{-1}
Single vent	B2 (Bottom full open)	1 hour after ventilation	4.80
	T2 (Top full open)	1 hour after ventilation	7.10
	R2 (Back roof full open)	1 hour after ventilation	4.20
Dual vents	B2+T2 (Bottom full+Top full)	1 hour after ventilation	7.20
	T2+R2 (Top full+Back roof full)	1 hour after ventilation	5.30
	B2+R2 (Bottom full+Back roof full)	1 hour after ventilation	5.30
All vents open	B2+T2+R2 (All three vents full open)	1 hour after ventilation	10.40
Rate comparison over time	T1+R2 (Top half+Back roof full)	12:00-13:00	3.06
		13:00-16:00	/
	B2+R1 (Bottom full+Back roof half)	12:00-13:00	0.08
		13:00-16:00	0.86
	B1+R2 (Bottom half+Back roof full)	12:00-13:00	1.05
		13:00-16:00	0.25
	B1+T2 (Bottom half+Top full)	12:00-13:00	2.86
		13:00-16:00	0.50

Greenhouse ventilation management requires dynamic decision-making. It is suggested that managers flexibly select appropriate schemes based on real-time monitored indoor and outdoor environmental parameters. For example, starting with the extreme cooling scheme in the afternoon and then switching to the balanced cooling scheme for maintenance can realize safe, efficient, and energy-saving control of the greenhouse environment in summer.

During the experimental design phase, this study fully considered adaptability to practical application scenarios. To address potential limitations, the applicable boundaries of the research have been clearly defined: the ventilation schemes proposed in this study are mainly applicable to low-growing crops or seedling raising scenarios where the crop height does not exceed 1.5 m and the canopy coverage is relatively low. For tall crops or high-density planting scenarios, further verification and adjustment are required according to the actual canopy characteristics.

4 Conclusions

This study proposed a novel ventilation system suitable for newly assembled CSGs, with top vents as the main ventilation component, bottom vents as supplementary ventilation, and back roof vents as auxiliary ventilation. Based on wireless temperature and humidity sensors, the effects of different vents, opening areas, and ventilation durations on the cooling effect were quantified through field measurements. The main conclusions are as follows:

1) A WSN platform was established, and with the support of OK interpolation, LabVIEW software was used to realize the visualization of real-time temperature distribution, improving the method for real-time temperature monitoring and analysis in CSGs.

2) In the test of different vent combinations, when only one vent was open, the temperature reductions of B2, T2, and R2 were 4.8°C, 7.1°C, and 4.2°C, respectively, with the cooling rate of T2 being 2.3 and 2.9°C/h higher than that of B2 and R2. When two vents were open, the indoor temperature reductions of B2+T2, T2+R2, and B2+R2 were 7.2°C, 5.3°C, and 5.3°C, respectively. When all vents were fully open, the temperature reduction of B2+T2+R2 reached 10.4°C, achieving the best cooling effect.

3) With more vents open, the increase in ventilation area had a more pronounced effect on enhancing the cooling effect and a more significant impact on the uniformity of indoor airflow distribution.

4) The cooling rates under different ventilation durations varied significantly. B1+T2 and B1+R2 achieved the best cooling effects in summer, with cooling rates typically being fast in the early stage and slow in the later stage.

This study adopted a field measurement method, which, compared with the CFD simulation method commonly used to evaluate the ventilation effect of CSGs, can be applied to different structural types of CSGs and can real-time locate environmental anomalies in the internal environment of greenhouses. The feasibility of the WSN platform for studying CSG ventilation and cooling was verified, and the results of this study will provide a reference for farmers to control ventilation systems and offer basic data support for the intelligent decision-making of novel CSG ventilation systems in the future.

Acknowledgements

This work was financially supported by Open Project of Key Laboratory of the Ministry of Agriculture and Rural Affairs (Grant No. 202201), Independent Research and Development Plan of Academy of Agricultural Planning and Engineering, MARA (Grant No. SH202402), Agricultural Planning Talent Project of Academy of Agricultural Planning and Engineering, MARA (Grant No. QNYC-2024-10), and Key R & D Program of Shaanxi Province (Grant No. 2025NC-YBXM-195).

[References]

[1] Food and Agriculture Organization of the United Nations. Food production must increase by 70% by 2050 to feed an additional 2.3 billion people. Available: https://www.fao.org/home/zh. Accessed on: [2024-03-15].

[2] Oliveira W, Colares L F, Porto R G, Viana B F, Tabarelli M, Lopes A V. Food plants in Brazil: Origin, economic value of pollination and pollinator shortage risk. Science of The Total Environment, 2024; 912: 169147.

[3] Qasim W, Xia L L, Lin S, Wan L, Zhao Y M, Butterbach-Bahl K. Global greenhouse vegetable production systems are hotspots of soil N_2O emissions and nitrogen leaching: A meta-analysis. Environmental Pollution, 2021; 272: 116372.

[4] National Bureau of Statistics. Agricultural development is advancing in strides, and modern agriculture is writing a new chapter-the second in a series of reports on the achievements of China's economic and social development over the past 75 years. Available: https://www.stats.gov.cn/sj/sjjd/202409/t20240910_1956334.html. Accessed on: [2024-03-15]

[5] Guo Y, Zhao H J, Zhang S H, Wang Y, Chow D. Modeling and optimization of environment in agricultural greenhouses for improving cleaner and sustainable crop production. Journal of Cleaner Production, 2021; 285: 124843.

[6] Li A, Huang L, Zhang T. Field test and analysis of microclimate in naturally ventilated single-sloped greenhouses. Energy and Buildings, 2017; 138: 479–489.

[7] Muñoz-Liesa J, Royapoor M, Cuerva E, Gassó-Domingo S, Gabarrell X, Josa A. Building-integrated greenhouses raise energy co-benefits through active ventilation systems. Building and Environment, 2022; 208: 108585.

[8] Zhang W. Simulation study on energy saving operation of solar greenhouse ventilation based on EnergyPlus. Master's thesis. Tai'an: Shandong Agricultural University, 2022; 5. 79 p. (in Chinese)

[9] Xue X P, Su W. CFD simulation of humidity distribution in solar greenhouse under natural ventilation. Journal of Marine Meteorology, 2019; 39(4): 90–96. (in Chinese)

[10] Akrami M, Javadi A A, Hassanein M J, Farmani R, Dibaj M, Tabor G R, Negm A. Study of the effects of vent configuration on mono-span greenhouse ventilation using Computational Fluid Dynamics. Sustainability, 2020; 12(3): 986.

[11] Benni S, Tassinari P, Bonora F, Barbaresi A, Torreggiani D. Efficacy of greenhouse natural ventilation: Environmental monitoring and CFD simulations of a study case. Energy and Buildings, 2016; 125: 276–286.

[12] He K S, Sun L, Huang Z Y, Liu Z L, Chen D Y. Optimization of vent configuration for ventilation dehumidification in multi-span plastic greenhouses. Transactions of the CSAM, 2012; 43(11): 186–191. (in Chinese)

[13] Zhao P. Simulation and experimental study of indoor environment of solar greenhouse under natural ventilation conditions. Master's dissertation. Jinan: Shandong Jianzhu University, 2021; 6. 73p. doi: 10.27273/d.cnki.gsajc.2021.000461. (in Chinese)

[14] Villagrán E A, Baeza Romero E J, Bojacá C R. Transient CFD analysis of the natural ventilation of three types of greenhouses used for agricultural production in a tropical mountain climate. Biosystems Engineering, 2019; 188: 288–304.

[15] Lyu X, Xu Y Q, Wei M, Wang C Q, Zhang G S, Wang S J. Effects of vent opening, wind speed, and crop height on microenvironment in three-span arched greenhouse under natural ventilation. Computers and Electronics in Agriculture, 2022; 201: 107326.

[16] Zhao R S. Influence of different ventilation conditions on airflow and temperature and humidity in plastic greenhouse. Master's dissertation. Yangling: Northwest A&F University, 2021; 6. 51p. (in Chinese)

[17] Luo H J. Applications of ANSYS/FLOTRAN in mechanically ventilated multispan plastic greenhouse. Master's dissertation. Wuhan: Huazhong Agricultural University, 2008; 6. 67p. (in Chinese)

[18] Zhang Y M, Liu C Q, Zhang H L, Liang C Y. CFD analysis of flow field for cold region rice seedlings greenhouse under natural ventilation condition. Journal of Agricultural Mechanization Research, 2018; 40(7): 19–23. (in Chinese)

[19] Zhang Y M. Numerical simulation analysis and research of the cold rice

seedling greenhouse environment based on CFD. Master's dissertation. Daqing: Heilongjiang Bayi Agricultural University, 2018; 6. 63p.

[20] Cheng X H, Mao H P, Ni J. Numerical prediction and CFD modeling of relative humidity and temperature for greenhouse-crops system. Transactions of the CSAM, 2011; 42(2): 173–179. (in Chinese)

[21] He X L, Wang J, Guo S R, Zhang J, Wei B, Sun J, et al. Ventilation optimization of solar greenhouse with removable back walls based on CFD. Computers and Electronics in Agriculture, 2018; 149: 16–25.

[22] Yan L L, Jing H W, Bao E C, Cao Y F, Pan T H, Shen T T, et al. Effects of different natural ventilation methods on the performance of solar greenhouse. Journal of China Agricultural University, 2020; 25(3): 71–78. (in Chinese)

[23] Teitel M, Liran O, Tanny J, Barak M. Wind driven ventilation of a mono-span greenhouse with a rose crop and continuous screened side vents and its effect on flow patterns and microclimate. Biosystems Engineering, 2008; 101(1): 111–122.

[24] Santolini E, Pulvirenti B, Benni S, Barbaresi L, Torreggiani D, Tassinari P. Numerical study of wind-driven natural ventilation in a greenhouse with screens. Computers and Electronics in Agriculture, 2018; 149: 41–53.

[25] Zhao J Q, Zhao Y. Computational fluid dynamics simulation on temperature field of mechanical ventilation for multi-span greenhouse. Journal of Chinese Agricultural Mechanization, 2014; 35(6): 76–79. (in Chinese)

[26] Cheng X, Huang Y Y, Ren H Y, Ren Z H. Simulation of summer mechanical ventilation in flower greenhouses based on CFD. Journal of Hebei Agricultural University, 2021; 44(5): 113–118. (in Chinese)

[27] Zheng M J, Mao H P. CFD analysis about effect of plant height on natural ventilation in greenhouse. Journal of Agricultural Mechanization Research, 2016; 38(5): 20–23,27. (in Chinese)

[28] Liu J R, Wen X Z, Li Y L, Bai J Y. Effect of the wall of solar greenhouse with forced ventilation on the indoor temperature and humidity. Journal of Shanxi Agricultural Sciences, 2018; 46: 421–425. (in Chinese)

[29] Ren S G, Yang W, Wang H Y, Xue W, Xu H L, Xiong Y J. Prediction model on temporal and spatial variation of air temperature in greenhouse and ventilation control measures based on CFD. Transactions of the CSAE, 2015; 31(13): 207–214. (in Chinese)

[30] Zhou C J. Dr. Zhou's investigation of picking zero (129) daylight greenhouse roof ridge film ventilation system - Gansu facility agricultural inspection documentary (5). Agricultural Engineering Technology, 2022; 42(16): 42–44,48. (in Chinese)

[31] Chinese government website. Opinions of the Ministry of Agriculture and Rural Affairs on accelerating the mechanization of planting facilities. Available: https://www.gov.cn/zhengce/zhengceku/2020-06/30/content_5522757.htm. Accessed on: [2024-03-15]

[32] Jiao W, Liu Q, Gao L J, Liu K Y, Shi R, Ta N. Computational fluid dynamics-based simulation of crop canopy temperature and humidity in double-film solar greenhouse. Journal of Sensors, 2020; 2020(1): 8874468.

[33] Tong G, Christopher D M, Li B. Numerical modelling of temperature variations in a Chinese solar greenhouse. Computers and Electronics in Agriculture, 2009; 68(1): 129–139.

[34] Caicedo-Ortiz J G, De-la-Hoz-Franco E, Morales Ortega R, Piñeres-Espitia G, Combita-Niño H, Estévez F, et al. Monitoring system for agronomic variables based in WSN technology on cassava crops. Computers and Electronics in Agriculture, 2018; 145: 275–281.

[35] Gulati K, Kumar Boddu R S, Kapila D, Bangare S L, Chandnani N, Saravanan G. A review paper on wireless sensor network techniques in Internet of Things (IoT). Materials Today: Proceedings, 2022; 51: 161–165.

[36] Oussama G, Rami A, Tarek F, Alanazi A S, Abid M. Fast and intelligent irrigation system based on WSN. Computational Intelligence and Neuroscience, 2022; 2022(1): 5086290.

[37] Al Qundus J, Dabbour K, Gupta S, Meissonier R, Paschke A. Wireless sensor network for AI-based flood disaster detection. Annals of Operations Research, 2022; 319(1): 697–719.

[38] Lv H H, Niu Y Y, Han Y X, Li S D, Zhang M, Li H. Spatiotemporal variation of crop-canopy light intensity and air temperature and humidity in summer solar greenhouse. Transactions of the CSAM, 2024; 55(5): 368–378. (in Chinese)

[39] Yang S Y, Liu X, Liu S Y, Chen X Y, Cao Y F. Real-time temperature distribution monitoring in Chinese solar greenhouse using virtual Lan. Agronomy, 2022; 12(7): 1565.

[40] Xia T Y, Li Y M, Sun Z P, Wan X C, Sun D P, Wang L, et al. Performance study of an active solar water curtain heating system for Chinese solar greenhouse heating in high latitudes regions. Applied Energy, 2023; 332: 120548.

[41] Huang W. Research on the ventilation control of daylight greenhouses in bitter saltwater desalination system. Master's thesis. Jinan: Shandong University of Architecture, 2023; 6. 65 p. doi: 10.27273/d.cnki.gsajc.2023.000169. (in Chinese)